

Hamiltonian learning with real-space impurity tomography in topological moiré superconductors

Maryam Khosravian,^{1,*} Rouven Koch,^{1,*} and Jose L. Lado¹

¹*Department of Applied Physics, Aalto University, 02150 Espoo, Finland*

Extracting Hamiltonian parameters from available experimental data is a challenge in quantum materials. In particular, real-space spectroscopy methods such as scanning tunneling spectroscopy allow probing electronic states with atomic resolution, yet even in those instances extracting the effective Hamiltonian is an open challenge. Here we show that impurity states in modulated systems provide a promising approach to extracting non-trivial Hamiltonian parameters of a quantum material. We show that by combining the real-space spectroscopy of different impurity locations in a moiré topological superconductor, modulations of exchange and superconducting parameters can be inferred via machine learning. We demonstrate our strategy with a physically-inspired harmonic expansion combined with a fully-connected neural network that we benchmark against a conventional convolutional architecture. We show that while both approaches allow extracting exchange modulations, only the former approach allows inferring the features of the superconducting order. Our results demonstrate the potential of machine learning methods to extract Hamiltonian parameters by real-space impurity spectroscopy as local probes of a topological state.

INTRODUCTION

Learning Hamiltonian parameters from experimental data is one of the most critical open problems in order to bring together experiments with theoretical models[1–8]. Conventionally, phenomenological models to account for experimental data are developed on a case by case basis. In certain instances, obtaining the Hamiltonian parameters of the model can be done by fitting specific features of the data[9, 10]. Many-body Hamiltonians with local interactions can be extracted local observables by exploiting time evolution and quantum Hamiltonian tomography, a strategy demonstrated theoretically and experimentally[11–16]. However, in some instances, no simple fitting procedure nor time-dependent measurements can be performed to extract Hamiltonian parameters. Machine learning methods have risen as a powerful approach to extract subtle features of data, and in particular they have become successful in tackling inverse problems in quantum materials[17–28].

Van der Waals heterostructures are a paradigmatic system in which, thanks to their tunability, a variety of quantum Hamiltonians can be emulated[29]. Specifically, the capability of combining two-dimensional materials with radically different properties allows engineering systems simultaneously hosting antagonist order[30, 31], with the paradigmatic example of van der Waals heterostructures combining 2D magnets and superconductors[32–36]. Beyond the different coexisting orders, van der Waals materials bring a unique feature to heterostructures, the emergence of a moiré pattern[37–41]. The moiré pattern stems from the structural modulation in real space due to a twist angle between lattices. Most importantly, the moiré modulation leads to a spatial modulation of all the Hamiltonian parameters. This modulation is the driving force behind a variety of phenomena, including topological and correlated states

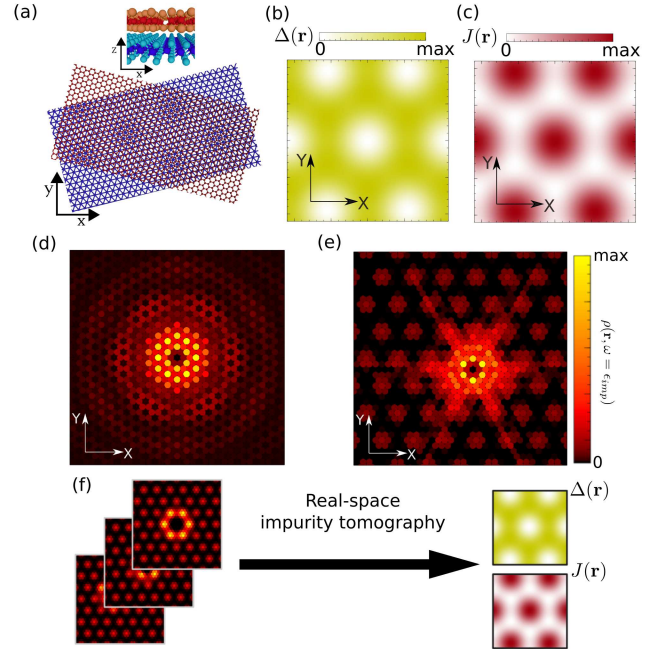


FIG. 1. Schematic of the moiré system (a), where panel (b) denotes the modulation of the superconducting and (c) the modulation of the exchange parameters. In the absence of moiré, impurities induced in-gap states in the topological superconducting state (d), which upon the existence of the moiré pattern gives rise to an interference effect (e). Using the spectroscopy of impurities in different locations, a machine learning algorithm extracts the exchange and superconducting profiles (f).

in van der Waals heterostructures[42–54]. However, extracting the values of these modulations in moiré system is an open problem, as their effect on the electronic structure is greatly challenging to disentangle. Interestingly, the coexistence of a moiré pattern and local impurities opens up a new strategy to infer electronic parameters

due to their non-trivial interplay[55–59].

In our manuscript, we put forward a method to extract Hamiltonian parameters of unconventional moiré superconductors using machine learning and impurity engineering. Specifically, we show that thanks to the moiré pattern, local impurities give rise to dramatically different electronic excitations depending on the location of the moiré pattern. This dependency allows us to directly infer moiré modulations via a machine learning algorithm that takes as input excitations for different impurity locations. We demonstrate that our algorithm allows extracting modulation strengths of exchange proximity and superconducting order, two parameters that cannot be directly extracted from a measured local density of states. We further address the robustness of our algorithm to noise, showing that Hamiltonian parameters can be extracted in an experimentally realistic scenario.

METHODS

Model

We consider an artificial two-dimensional superconductor obtained by combining a two-dimensional ferromagnet and a two-dimensional superconductor[32–34] as shown in Fig. 1a. The electronic structure of the heterostructure is modeled with an atomistic Wannier orbital site forming a triangular lattice, where the moiré pattern is incorporated in the modulation of the Hamiltonian parameters[60–64]. The full Hamiltonian takes the form

$$\mathcal{H}_0 = \mathcal{H}_{\text{kin}} + \mathcal{H}_J + \mathcal{H}_R + \mathcal{H}_{\text{SC}} \quad (1)$$

with $\mathcal{H}_{\text{kin}} = t \sum_{\langle ij \rangle, s} c_{i,s}^\dagger c_{j,s} + \mu \sum_i c_{i,s}^\dagger c_{i,s}$ with $c_{n,s}^\dagger$ ($c_{n,s}$) the creation (annihilation) fermionic operator with spin s in site n . The combination of exchange coupling, Rashba spin-orbit coupling and superconducting proximity gives rise to topological superconducting state when combined on the right footing[32, 65–70]. We focus on the regime giving rise to topological superconducting states $C = 1, 2, 3$, which arise when taking the chemical potential crossing the Γ, K, M points, respectively. The hopping is controlled by t , the chemical potential by μ and $\langle i, j \rangle$ runs over nearest neighbors. The term $\mathcal{H}_R = i\lambda_R \sum_{\langle ij \rangle, ss'} \mathbf{d}_{ij} \cdot \boldsymbol{\sigma}^{s,s'} c_{i,s}^\dagger c_{j,s'}$ is the Rashba spin-orbit coupling arising from mirror symmetry breaking at the interface[71], with $\boldsymbol{\sigma}$ the spin Pauli matrices, λ_R controls the spin-orbit coupling constant and $\mathbf{d}_{ij} = (\mathbf{r}_i - \mathbf{r}_j) \times \hat{z}$.

We now focus on the main terms that we will extract with our procedure, the modulated exchange and modulated superconductivity. The exchange coupling is included in a term

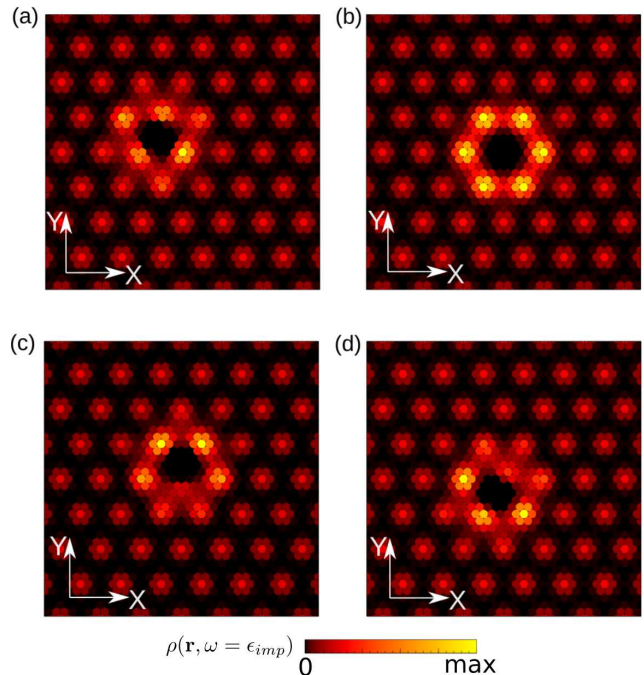


FIG. 2. Local density of states of the in-gap state for a single impurity in a moiré topological superconductor for different impurity locations (a-d). It is observed that depending on the location of the impurity in the moiré, the in-gap states show different interference patterns with the moiré potential. These different interference patterns reflect the underlying modulations of the Hamiltonian, and allow us to extract Hamiltonian modulation from real-space spectroscopy. In the absence of the moiré pattern, all the impurity locations would show the same profile of the in-gap state.

$$\mathcal{H}_J = \sum_{i,s,s'} J(\mathbf{r}) \sigma_z^{s,s'} c_{i,s}^\dagger c_{i,s'} \quad (2)$$

and the superconducting order by

$$\mathcal{H}_{\text{SC}} = \sum_i \Delta(\mathbf{r}) c_{i,\uparrow}^\dagger c_{i,\downarrow}^\dagger + h.c. \quad (3)$$

where $J(\mathbf{r})$ and $\Delta(\mathbf{r})$ parameterize the exchange coupling and induced s-wave superconductivity. The competition between the exchange field and the superconducting order leads to an induced modulated superconductivity stemming from the originally modulated exchange[72–74]. We take a modulation parametrized as $f(\mathbf{r}) = c_0 + c_1 \sum_{n=1}^3 \cos(R^n \mathbf{q} \cdot \mathbf{r})$ where \mathbf{q} is the moiré superlattice wave vector, and R_n is the rotation matrix conserving C_3 symmetry. The parameters c_0, c_1 are defined so that $\langle f(\mathbf{r}) \rangle = 0$. The spatial profiles $J(\mathbf{r})$ and $\Delta(\mathbf{r})$ are written in terms of the previous spatial dependence as

$$\begin{aligned} J(\mathbf{r}) &= J_0 + \delta_J f(\mathbf{r}) \\ \Delta(\mathbf{r}) &= \Delta_0 + \delta_\Delta (1 - f(\mathbf{r})) \end{aligned} \quad (4)$$

J_0 and Δ_0 parametrize the average magnitude of the modulated exchange and superconducting profiles, whereas δ_J and δ_Δ control the amplitude of the moiré modulation. For the sake of concreteness we take $J_0 = \lambda_R$ and $\Delta_0 = \lambda_R/2$. The relative signs of $f(\mathbf{r})$ in $J(\mathbf{r})$ and $\Delta(\mathbf{r})$ are taken so that when the superconducting order is maximum, the exchange is minimum (Fig. 1bc).

Local non-magnetic impurities are included adding a potential scattering term of the form

$$\mathcal{H}_{\text{imp}} = W \sum_s c_{n,s}^\dagger c_{n,s} \quad (5)$$

where \mathcal{H}_{imp} defines the impurity Hamiltonian at site n with an on-site potential w . We focus on the strong impurity limit in which the site is effectively removed from the low energy manifold taking $W = 100t$. The full Hamiltonian of the defective system takes the form

$$\mathcal{H} = \mathcal{H}_0 + \mathcal{H}_{\text{imp}} \quad (6)$$

The impurity gives rise to an in-gap state both in the absence (Fig. 1d) and presence (Fig. 1(e)) of a moiré modulation. It is important to note that, due to the presence of the moiré pattern, the impact of an impurity depends on its location with respect to the moiré modulation. Specifically, as shown in the local density of states of Fig. 2, the interference between the impurity state and the moiré potential gives rise to different patterns depending on the location. This interference fully disappears when δ_J and δ_Δ are switched off. We will show that our machine learning algorithm will use the interference between the different locations of impurities to extract the values of the Hamiltonian modulations.

We finally elaborate on the computational procedure to solve this model in the limit of a single impurity in an otherwise pristine system. For this purpose, we will use Green's function embedding method.[75–77]. The embedding method relies on extracting the Green's function from the Dyson equation of the defective system

$$G_V(\omega) = [\omega - H_V - \Sigma(\omega) + i0^+]^{-1} \quad (7)$$

where $G_V(\omega)$ is the Green's function of the defective model, H_V the Hamiltonian of the defective unit cell, and $\Sigma(\omega)$ the selfenergy induced by the pristine system. The selfenergy $\Sigma(\omega)$ can be obtained from the Dyson equation for the pristine model $\Sigma(\omega) = \omega - H_0 - G_0(\omega)^{-1} + i0^+$ with H_0 the Hamiltonian of the pristine unit cell, where we take the Bloch's representation of the pristine unit

cell Green's function $G_0(\omega) = \frac{1}{(2\pi)^2} \int [\omega - H_{\mathbf{k}} + i0^+]^{-1} d^2\mathbf{k}$ where $H_{\mathbf{k}}$ is the Bloch's Hamiltonian.

The local density of states used as input for our algorithm is obtained as

$$\rho(\mathbf{r}, \omega) = -\frac{1}{\pi} \sum_{s,\tau} \langle \mathbf{r}, s, \tau | \text{Im}(G_V(\omega)) | \mathbf{r}, s, \tau \rangle \quad (8)$$

where s and τ are the spin and Nambu indexes. The in-gap state ϵ_{imp} is located using an iterative algorithm in the energy window of the topological superconducting gap. From an experimental point of view, a finite noise of the spectroscopy will be present, and thus the robustness of our algorithm will be important with regards to its experimental implementation. We emulate the impact of noise in the real-space spectroscopy as

$$\rho_{\text{noisy}}(\mathbf{r}) = \rho(\mathbf{r}) + \chi(\mathbf{r}) \quad (9)$$

adding a noise background $\chi(\mathbf{r}) = \chi_0 \cdot \mathcal{R}(\mathbf{r})$ to the local density of states (LDOS) $\rho(\mathbf{r})$ where χ_0 is the noise magnitude and $\mathcal{R}(\mathbf{r})$ is a random uniform noise distribution defined in the interval $(-\langle \rho(\mathbf{r}) \rangle, \langle \rho(\mathbf{r}) \rangle)$ with $\langle \rho(\mathbf{r}) \rangle$ as mean value of the LDOS.

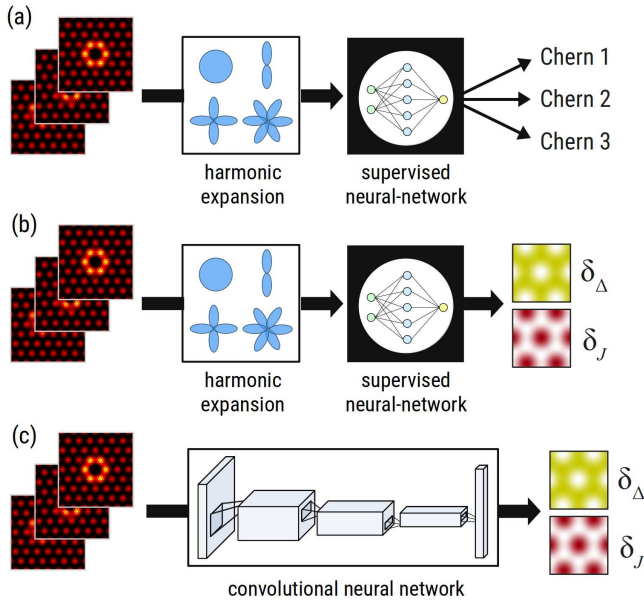
Machine Learning

The main idea of our real-space impurity tomography is to extract the underlying Hamiltonian by using the LDOS for different impurity positions as inputs as shown in Fig. 1(f). The extraction of the superconducting and exchange modulation is a non-trivial problem without a simple one-to-one correspondence to a single real-space spectroscopy.

We will use a physics-inspired approach to compress the information contained in the LDOS with a harmonic expansion (see Fig. 3(ab)). The coefficients of the power spectrum for each LDOS are then concatenated and fed into a fully-connected neural network (NN) as depicted in Fig. 3(b). The radial expansion works as follows. First, each individual LDOS is centered around the impurity position. Then, the harmonic expansion for the power spectrum is performed as

$$c_{ln} = \sum_{\alpha} \rho(\mathbf{r}_{\alpha}) e^{il\phi_{\alpha}} r_{\alpha}^n e^{-r_{\alpha}/\Lambda} \quad (10)$$

where c_{ln} are the coefficients of the expansion, $\mathbf{r}_{\alpha} = r_{\alpha}(\cos \phi_{\alpha}, \sin \phi_{\alpha}, 0)$ the atomic sites taking as the origin the impurity site, and Λ is the typical localization length of the state.[78] In particular, we expand each LDOS into 24 complex c_{ln} coefficients, i.e. the input dimension of the NN is 144 after concatenating the real and imaginary components of the coefficients for three LDOS. We



first train a fully-connected NN to perform classification of the Chern number of a given LDOS image which is compressed again into radial functions. The workflow is shown in Fig. 3(a). The NN architecture is shown in Table I. The loss function for this case is the *categorical crossentropy loss* and a *softmax-activation function* is used for the output layer. The training consists of 100 epochs, with a batch size of 16. The optimization is performed with the Adam optimizer and a learning rate of 0.001. Afterward, we create a supervised architecture to predict the Hamiltonian parameter of the exchange and superconducting modulation (δ_J, δ_Δ). For this regression task, the architecture of the NN is shown in Table II. We trained the NN for 100 epochs with a batch size of 16. For the optimization of the weights, we are using the stochastic gradient descent algorithm and the Adam optimizer [79] with a learning rate of 0.001. The loss function is the mean squared error (MSE). For the training and testing, we created LDOS for 2000 Hamiltonians for each Chern number where we varied the parameter $\delta_J \in [0, 2\lambda_R]$ and $\delta_\Delta \in [0, \lambda_R]$. This results in 6000 samples which we divided into a training set of 5400 and a test set of 600 examples. Finally, we take as a benchmark of our procedure a convolutional neural network (CNN) [80] architecture. We take an analogous workflow as shown in Fig. 3(c), where three LDOS with different impurity positions are fed into the CNN which

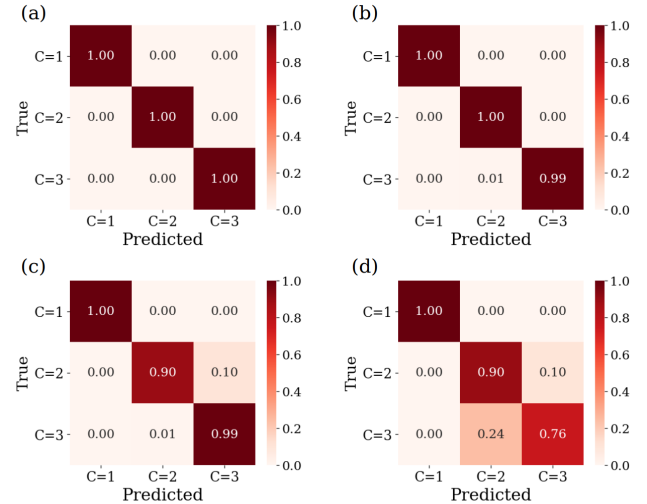


FIG. 4. Extraction of the Chern number. Panels (a) and (b) show the prediction accuracy of $C=1,2,3$ when using three impurity positions as input for the NN for zero noise (a) and the maximum noise amplitude (b). Panels (c) and (d) show the prediction accuracy of $C = 1, 2, 3$ when using one impurity position as input for the NN for zero noise (c) and the maximum noise amplitude (d).

predicts the modulation of the exchange or superconductivity as a regression task. The architecture of the CNN is shown in Table III, where three CNN networks are concatenated into a fully-connected NN and trained simultaneously with three input LDOS. For the training, we used 50 epochs with a batch size of 16.

It is finally worth noting that our machine learning approach allows us to exploit the spatial resolution of scanning tunneling microscopy. In the case of unconventional superconductors, the non-trivial interference between bound states provides information about the underlying electronic state, information that is often not accessible with other probes. Other approaches to Hamiltonian learning use the energy and entanglement spectra for Hamiltonian inference[81], or employing time-resolved measurements to extract Hamiltonian parameters [7]. However, performing those measurements for unconventional superconductors is greatly challenging, whereas the measurements of the local density of states in our impurity tomography approach are standard in scanning probe experiments in two-dimensional superconductors.

RESULTS AND DISCUSSION

Chern number extraction

The first problem we tackle is to determine the Chern number from one or three LDOS with different impurity locations. The measurement of topological invari-

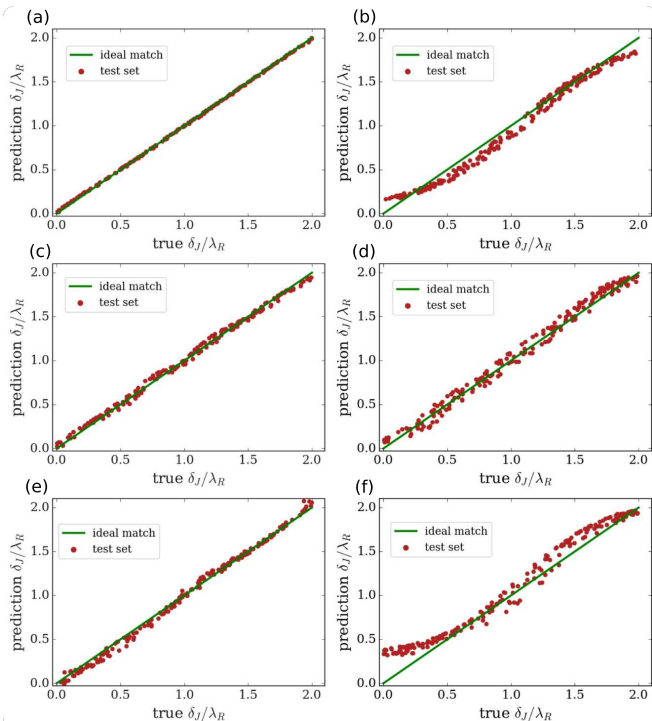


FIG. 5. Predictions of δ_J with a harmonic expansion fully-connected architecture (a,c,e) compared to the convolutional architecture predictions (b,d,f) for Chern numbers $C = 1$ (a,b), $C = 2$ (c,d), and $C = 3$ (e,f). It is observed that the harmonic expansion fully-connected architecture provides slightly more accurate predictions than the convolutional architecture.

ants in topological superconductors is a practical open challenge[82–87], as due to their topological nature, local order parameters cannot be defined for these states. The appearance of in-gap modes alone is not enough to assess the topological invariant of a superconductor, as in-gap states can appear in both trivial and topological superconductors[88]. Interestingly, the inclusion of a moiré pattern leads to subtle changes in the spatial distribution of in-gap states[55]. As we will show below, the fine structure of the in-gap modes allows for extracting the topological invariant of the underlying state.

In the following, we elaborate on the procedure to extract the topological invariant solely from the real-space spectroscopy images of single impurities. The input of the algorithm consists of the real-space spectroscopy for three impurity locations, and its output is the topological invariant. To extract the topological invariant, we trained a NN to perform the classification into the 3 non-trivial Chern numbers. The results are shown in Fig. 4 in the form of confusion matrices for three Fig. 4(a,b) and one LDOS Fig. 4(c,d) as input. For one LDOS as input, we achieve an average accuracy of 96.3% for the test data with zero noise (c) and 88.7% with the maximum noise amplitude of $\chi_0 = 0.4$. The confusion matrix

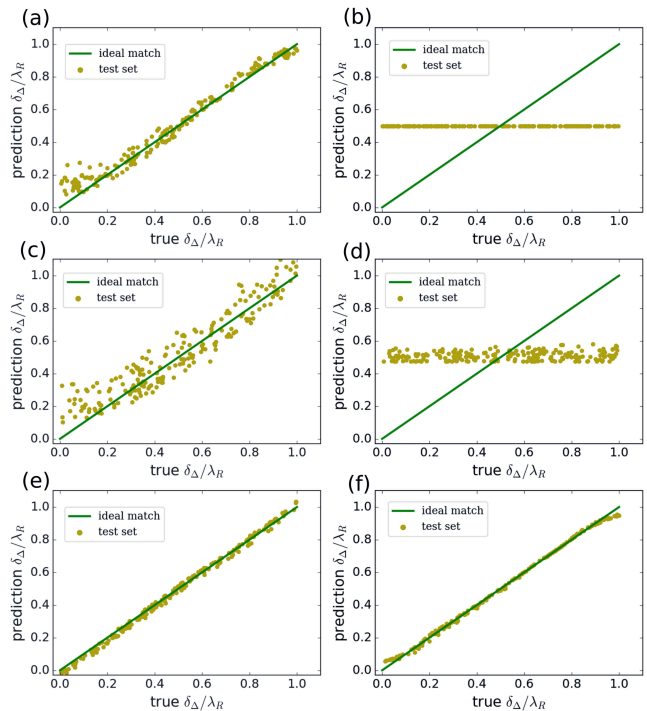


FIG. 6. Predictions of δ_Δ with a harmonic fully-connected architecture (a,c,e) compared to a convolutional architecture (b,d,f) for Chern numbers $C = 1$ (a,b), $C = 2$ (c,d), and $C = 3$ (e,f). It is observed that the harmonic fully-connected architecture provides more accurate predictions than the convolutional architecture, in particular for $C = 1, 2$ where the convolutional architecture fails.

shows that $C = 1$ can be predicted with 100% accuracy in both cases, the NN is only confused in the prediction between $C = 2$ and $C = 3$. Taking three real-space spectroscopies with different impurity positions as input, we obtain a testing accuracy of 100% for zero noise (a) and 99.7% for the maximum noise amplitude. This highlights that combining three real-space spectroscopies for different impurity locations substantially increases the accuracy of the topological invariant predictions. These results show, that it is possible to extract the Chern number by just one LDOS with a random impurity position even in the case of very noisy data.

Exchange field extraction

In the following, we show how the real-space impurity tomography allows extracting the values of the moiré Hamiltonian parameters. We start with the modulation of the exchange coupling, which is intuitively the parameter that will impact the real-space spectroscopy in the strongest way. This stems from the fact that the local exchange coupling creates in-gap Yu-Shiba-Rusinov modes inside the original superconducting gap Δ [32, 34, 89–95], and these modes form the low energy electronic

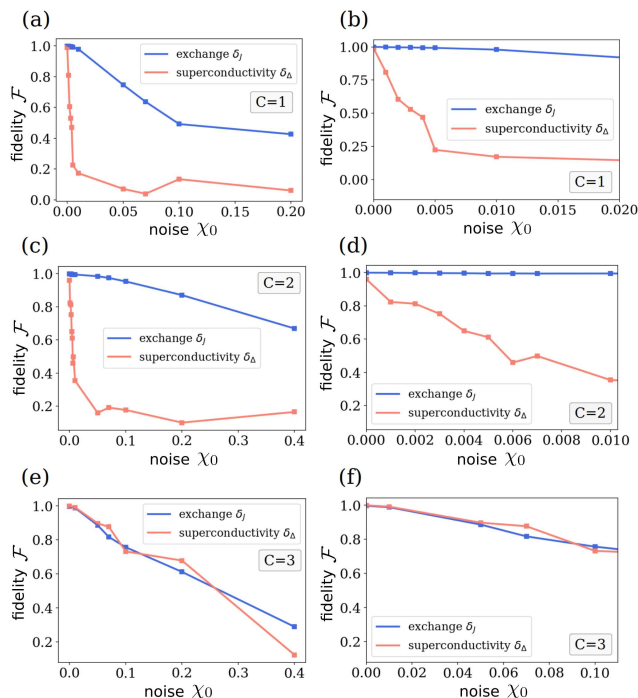


FIG. 7. Analysis of the correlation between the predicted and real values of the exchange and superconducting modulation as a function of the noise level for $C = 1$ (a,b), $C = 2$ (c,d), and $C = 3$ (e,f). Panels (a,c,e) correspond to a larger noise range, whereas (b,d,f) correspond to the low noise limit. It is observed that exchange modulations δ_J are more resilient to noise than superconducting modulation predictions δ_Δ .

structure leading to a topological superconducting state. As a result, low energy bands reflect the periodicity of the exchange modulation, and their associated in-gap modes in the presence of impurities inherit the same dependence[34, 77].

We take as input the real-space spectroscopy for three impurity locations, leading as output the modulation strength of the exchange coupling in the system. We train different architectures for each Chern number, including convolutional neural networks of the full spectroscopy and the harmonic expansion of the impurity states. The results, shown in Fig. 5 demonstrate that real-space spectroscopy of the impurities allows extracting the modulation of the exchange coupling with both procedures. Specifically, it is shown that both convolutional and harmonic expansion obtain a substantial accuracy in the extraction, specifically leading to a typical error of $\mathcal{E}[\delta_J] = 0.01$ for the convolutional algorithm and $\mathcal{E}[\delta_J] = 0.0072$ for the harmonic expansion. We observe that the harmonic algorithm becomes slightly more accurate than the convolutional method. Interestingly, the difference between both methods becomes much more dramatic in the extraction of superconducting order values and modulations.

Superconducting order extraction

We now move to consider the extraction of the local superconducting order $\Delta(\mathbf{r})$ with real-space impurity tomography. It is interesting to note that the impact of modulation of Δ in the low energy states is expected to be more subtle than the exchange. While the energy location of a Yu-Shiba-Rusinov strongly depends on J , the value of the superconducting gap only leads to proportional renormalization of the energy[88].

We show in Fig. 6 the extraction of the superconducting modulation using the harmonic expansion with supervised learning (Fig. 6(ace)) and the convolutional neural network architecture (Fig. 6(bdf)), for $C = 1$ (Fig. 6(ab)), $C = 2$ (Fig. 6(cd)) and $C = 3$ (Fig. 6(ef)). In the case $C = 3$ (Fig. 6(ef)), we observe that both architectures are capable of predicting the superconducting modulation. Interestingly, for $C = 1$ (Fig. 6ab) and $C = 2$ (Fig. 6cd), the convolutional architecture is incapable of predicting correct superconducting modulations, whereas the fully-connected harmonic expansion successfully predicts it. Typical errors of the NNs are $\mathcal{E}[\delta_\Delta] = 0.30, 0.29, 0.008$ for $C = 1, 2, 3$ for CNN and $\mathcal{E}[\delta_\Delta] = 0.03, 0.024, 0.008$ for $C = 1, 2, 3$ for harmonic expansion with the fully-connected NN. This phenomenology should be contrasted with the exchange modulation, where both architectures showed similar performance. The success of the fully-connected harmonic expansion and failure the CNN architecture demonstrates that the extraction of superconducting modulations represents a much more challenging problem than the exchange modulation. In particular, our harmonic expansion shows that such a physically-motivated procedure allows extracting Hamiltonian parameters stemming from highly subtle changes in the real-space spectroscopy.

Noisy Hamiltonian extraction

In the following, we address the extraction of the Hamiltonian in the presence of noisy data. For the sake of concreteness, we focus on the harmonic fully-connected architecture, as the superconducting modulation can be predicted with that one. We show in Fig. 7 the evolution of the correlation between predictions and true values as a function of increasing noise. We define prediction fidelity as

$$\mathcal{F}(\delta^{pred}, \delta^{true}) = \frac{|\langle \delta^{pred} \delta^{true} \rangle - \langle \delta^{true} \rangle \langle \delta^{pred} \rangle|}{\sqrt{(\langle (\delta^{true})^2 \rangle - \langle \delta^{true} \rangle^2)(\langle (\delta^{pred})^2 \rangle - \langle \delta^{pred} \rangle^2)}} \quad (11)$$

is defined in the interval $\mathcal{F} \in [0, 1]$, where $\mathcal{F} = 1$ corresponds to the best prediction accuracy $\delta^{pred} = \delta^{true}$

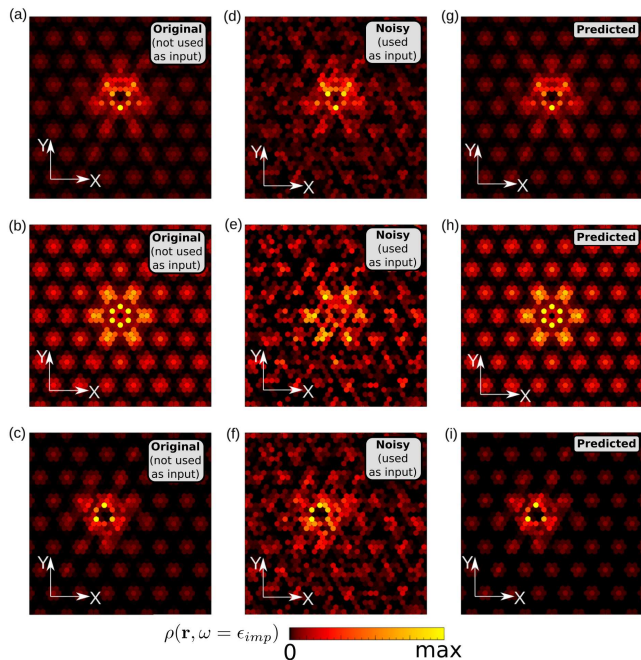


FIG. 8. Local density of states of the in-gap state for a single impurity in a moiré superlattice with $C = 3$ for three different locations for (a)-(c). Panels (d)-(f) show the real-space spectroscopy with $\chi_0 = 0.2$ noise amplitude, which is used as input for the machine learning algorithm. Panels (g)-(i) show the real-space spectroscopy associated to the predicted Hamiltonian by the neural network.

and $\mathcal{F} = 0$ corresponds to no predictive accuracy. Focusing first on the exchange modulation shown in Fig. 7, we observe that even substantial noise allows to infer the value of its modulation for the Chern numbers. The robustness of the exchange modulation extraction is consistent with the fact that the neural network architecture was capable of providing faithful predictions of the parameter. This resilience to noise stems from the strong dependence of the Yu-Shiba-Rusinov states on the local exchange, which directly impacts the real-space profile of the spectroscopy. The prediction of the superconducting modulation represents however a bigger challenge as shown in Fig. 7. In the cases $C = 1, 2$ (Fig. 7(abcd)), the most challenging ones, we observe that magnitudes of noise around $\chi_0 = 0.005$ break down the predictions. In stark contrast, systems with $C = 3$ are resilient to levels of noise magnitudes up to $\chi_0 = 0.2$ as shown in Fig. 7(ef). The difference in the robustness between $C = 1, 2$ and $C = 3$ can be rationalized by recalling that the convolutional neural network architecture is not capable of providing predictions for $C = 1, 2$, but it gave reliable predictions for $C = 3$. Interestingly, despite the superconducting modulation creating a very subtle impact in the real-space spectroscopy, our algorithm is capable of extracting the modulation amplitude from noisy data for different Chern numbers. Finally, we show in Fig. 8 a

comparison between the spectroscopies for the pristine data (Fig. 8abc), the noisy data provided as input to our algorithm (Fig. 8def) and the spectroscopy computed with the parameters predicted by the Hamiltonian extraction (Fig. 8ghi). It is observed that the spectroscopy predictions are nearly indistinguishable from the original ones, showing that our algorithm is capable of solving the inverse problem of inferring the Hamiltonian from the spectroscopy.

CONCLUSIONS

To summarize, we have shown that interference effects of in-gap states allow extracting Hamiltonian moiré parameters and topological invariants in an artificial topological superconductor from real-space spectroscopy patterns. Our approach is based on a supervised learning procedure that exploits the patterns obtained in in-gap states for different impurity locations simultaneously. We showed that our technique can be readily implemented with a convolution neural network architecture that combines several impurity locations simultaneously. Furthermore, we showed that by leveraging an orbital expansion of the impurity modes, a more robust machine-learning approach can be developed. Specifically, our procedure using a harmonic expansion is capable of extracting both parameter values and their modulations even in the presence of noise. We demonstrate that the combination of different locations dramatically increases the accuracy of Hamiltonian parameter inference, exemplifying how parameter inference benefits from features that our algorithm extracts from several impurity locations. Our results establish a machine learning methodology that exploits local impurity engineering to extract non-trivial parameters in artificial topological systems. Our demonstration exploits data directly accessible in scanning tunneling microscopy experiments and is robust in the presence of noise, establishing a realistic method to extract Hamiltonian parameters from readily accessible experimental data in complex quantum materials.

Acknowledgements: We acknowledge the computational resources provided by the Aalto Science-IT project, and the financial support from the Academy of Finland Projects Nos. 331342, 336243 and 358088, the Jane and Aatos Erkkö Foundation. We thank P. Liljeroth, S. Kezilebieke and T. Ojanen for useful discussions.

TABLE I. Architecture of the fully-connected NN of the expansion method. Used for the classification of the Chern number.

fully-connected NN (classification)		
Layer	Output shape	
harmonic expansion	<i>preprocessing</i>	
InputLayer	$(48 \cdot 3)$	<i>48 params / LDOS</i>
Dense	(200)	
Dropout	(200)	
Dense	(100)	
Dropout	(100)	
Dense	(20)	
Dropout	(20)	
Dense	(3)	
total parameters	51,183	

TABLE II. Architecture of the fully-connected NN of the expansion method. Used for the regression of the Hamiltonian parameters.

fully-connected NN (regression)		
Layer	Output shape	
harmonic expansion	<i>preprocessing</i>	
InputLayer	$(48 \cdot 3)$	<i>48 params / LDOS</i>
Dense	(300)	
Dropout	(300)	
Dense	(2)	
total parameters	15,302	

Appendix: Network Architectures

* These two authors contributed equally

- [1] James R. Garrison and Tarun Grover, "Does a single eigenstate encode the full hamiltonian?" *Phys. Rev. X* **8**, 021026 (2018).
- [2] Eli Chertkov and Bryan K. Clark, "Computational inverse method for constructing spaces of quantum models from wave functions," *Phys. Rev. X* **8**, 031029 (2018).
- [3] X. Turkeshi, T. Mendes-Santos, G. Giudici, and M. Dalmonte, "Entanglement-guided search for parent hamiltonians," *Phys. Rev. Lett.* **122**, 150606 (2019).
- [4] Rouven Koch and Jose L. Lado, "Designing quantum many-body matter with conditional generative adversarial networks," *Phys. Rev. Res.* **4**, 033223 (2022).
- [5] Agnes Valenti, Evert van Nieuwenburg, Sebastian Huber, and Eliska Greplova, "Hamiltonian learning for quantum error correction," *Phys. Rev. Res.* **1**, 033092 (2019).
- [6] Netta Karjalainen, Zina Lippo, Guangze Chen, Rouven Koch, Adolfo O. Fumega, and Jose L. Lado, "Hamiltonian inference from dynamical excitations in confined quantum magnets," *Phys. Rev. Appl.* **20**, 024054 (2023).
- [7] Liangyu Che, Chao Wei, Yulei Huang, Dafa Zhao, Shunzhong Xue, Xinfang Nie, Jun Li, Dawei Lu, and Tao Xin, "Learning quantum hamiltonians from single-qubit measurements," *Phys. Rev. Res.* **3**, 023246 (2021).
- [8] Kai Yang, Soo-Hyon Phark, Yujeong Bae, Taner Esat,

TABLE III. Architecture of the CNN. Used for the regression of the Hamiltonian parameters.

CNN		
Layer	Output shape	
combine three CNNs:		
InputLayer	(55,55,1)	
Conv2D	(55, 55, 32)	
MaxPooling2D	(27, 27, 32)	
Conv2D	(27, 27, 64)	
MaxPooling2D	(13, 13, 64)	
Flatten	(10816)	
fully-connected NN		
Concatenate	(32448)	<i>combine 3 CNNs</i>
Dense	(200)	
Dense	(50)	
Dense	(1) or (2)	
total parameters	6,556,349	

Philip Willke, Arzhang Ardavan, Andreas J. Heinrich, and Christopher P. Lutz, "Probing resonating valence bond states in artificial quantum magnets," *Nature Communications* **12** (2021), 10.1038/s41467-021-21274-5.

- [9] B. Bryant, A. Spinelli, J. J. T. Wagenaar, M. Gerrits, and A. F. Otte, "Local control of single atom magnetocrystalline anisotropy," *Phys. Rev. Lett.* **111**, 127203 (2013).
- [10] Shichao Yan, Deung-Jang Choi, Jacob A. J. Burgess, Steffen Rolf-Pissarczyk, and Sebastian Loth, "Three-dimensional mapping of single-atom magnetic anisotropy," *Nano Letters* **15**, 1938–1942 (2015).
- [11] Zhi Li, Lijun Zou, and Timothy H. Hsieh, "Hamiltonian tomography via quantum quench," *Phys. Rev. Lett.* **124**, 160502 (2020).
- [12] Eyal Bairey, Itai Arad, and Netanel H. Lindner, "Learning a local hamiltonian from local measurements," *Phys. Rev. Lett.* **122**, 020504 (2019).
- [13] Hsin-Yuan Huang, Yu Tong, Di Fang, and Yuan Su, "Learning many-body hamiltonians with heisenberg-limited scaling," *Phys. Rev. Lett.* **130**, 200403 (2023).
- [14] Agnes Valenti, Guliuxin Jin, Julian Léonard, Sebastian D. Huber, and Eliska Greplova, "Scalable hamiltonian learning for large-scale out-of-equilibrium quantum dynamics," *Phys. Rev. A* **105**, 023302 (2022).
- [15] Christian Kokail, Rick van Bijnen, Andreas Elben, Benoît Vermersch, and Peter Zoller, "Entanglement hamiltonian tomography in quantum simulation," *Nature Physics* **17**, 936–942 (2021).
- [16] Antonio A. Gentile, Brian Flynn, Sebastian Knauer, Nathan Wiebe, Stefano Paesani, Christopher E. Granade, John G. Rarity, Raffaele Santagati, and Anthony Laing, "Learning models of quantum systems from experiments," *Nature Physics* **17**, 837–843 (2021).
- [17] C. Di Franco, M. Paternostro, and M. S. Kim, "Hamiltonian tomography in an access-limited setting without state initialization," *Phys. Rev. Lett.* **102**, 187203 (2009).
- [18] Juan Carrasquilla, "Machine learning for quantum matter," *Advances in Physics: X* **5**, 1797528 (2020).
- [19] Sonia G. Schirmer and Daniel K. L. Oi, "Two-qubit hamiltonian tomography by bayesian analysis of noisy data," *Phys. Rev. A* **80**, 022333 (2009).
- [20] Luigi Seveso and Matteo G. A. Paris, "Estimation of gen-

- eral hamiltonian parameters via controlled energy measurements,” *Phys. Rev. A* **98**, 032114 (2018).
- [21] Ian Hincks, Christopher Granade, and David G Cory, “Statistical inference with quantum measurements: methodologies for nitrogen vacancy centers in diamond,” *New Journal of Physics* **20**, 013022 (2018).
- [22] Jianwei Wang, Stefano Paesani, Raffaele Santagati, Sebastian Knauer, Antonio A. Gentile, Nathan Wiebe, Maurangelo Petruzzella, Jeremy L. O’Brien, John G. Rarity, Anthony Laing, and Mark G. Thompson, “Experimental quantum hamiltonian learning,” *Nature Physics* **13**, 551–555 (2017).
- [23] Valentin Gebhart, Raffaele Santagati, Antonio Andrea Gentile, Erik M. Gauger, David Craig, Natalia Ares, Leonardo Banchi, Florian Marquardt, Luca Pezzè, and Cristian Bonato, “Learning quantum systems,” *Nature Reviews Physics* **5**, 141–156 (2023).
- [24] Rouven Koch, David van Driel, Alberto Bordin, Jose L. Lado, and Eliska Greplova, “Adversarial hamiltonian learning of quantum dots in a minimal kitaev chain,” *Phys. Rev. Appl.* **20**, 044081 (2023).
- [25] Faluke Aikebaier, Teemu Ojanen, and Jose L. Lado, “Extracting electronic many-body correlations from local measurements with artificial neural networks,” *SciPost Phys. Core* **6**, 030 (2023).
- [26] Faluke Aikebaier, Teemu Ojanen, and Jose L. Lado, “Machine learning the Kondo entanglement cloud from local measurements,” *arXiv e-prints*, arXiv:2311.07253 (2023), arXiv:2311.07253 [cond-mat.str-el].
- [27] Lukas J. Fiderer, Jonas Schuff, and Daniel Braun, “Neural-network heuristics for adaptive bayesian quantum estimation,” *PRX Quantum* **2**, 020303 (2021).
- [28] João Augusto Sobral, Stefan Obernauer, Simon Turkel, Abhay N. Pasupathy, and Mathias S. Scheurer, “Machine learning the microscopic form of nematic order in twisted double-bilayer graphene,” *Nature Communications* **14** (2023), 10.1038/s41467-023-40684-1.
- [29] Eva Y. Andrei, Dmitri K. Efetov, Pablo Jarillo-Herrero, Allan H. MacDonald, Kin Fai Mak, T. Senthil, Emanuel Tutuc, Ali Yazdani, and Andrea F. Young, “The marvels of moiré materials,” *Nature Reviews Materials* **6**, 201–206 (2021).
- [30] M. Gibertini, M. Koperski, A. F. Morpurgo, and K. S. Novoselov, “Magnetic 2d materials and heterostructures,” *Nature Nanotechnology* **14**, 408–419 (2019).
- [31] Yuan Liu, Nathan O. Weiss, Xidong Duan, Hung-Chieh Cheng, Yu Huang, and Xiangfeng Duan, “Van der waals heterostructures and devices,” *Nature Reviews Materials* **1** (2016), 10.1038/natrevmats.2016.42.
- [32] Shawulienu Kezilebieke, Md Nurul Huda, Viliam Vaňo, Markus Aapro, Somesh C. Ganguli, Orlando J. Silveira, Szczepan Głodzik, Adam S. Foster, Teemu Ojanen, and Peter Liljeroth, “Topological superconductivity in a van der waals heterostructure,” *Nature* **588**, 424–428 (2020).
- [33] Shawulienu Kezilebieke, Orlando J. Silveira, Md N. Huda, Viliam Vaňo, Markus Aapro, Somesh Chandra Ganguli, Jouko Lahtinen, Rhodri Mansell, Sebastiaan Dijken, Adam S. Foster, and Peter Liljeroth, “Electronic and magnetic characterization of epitaxial CrBr₃ monolayers on a superconducting substrate,” *Advanced Materials* **33**, 2006850 (2021).
- [34] Shawulienu Kezilebieke, Viliam Vaňo, Md N. Huda, Markus Aapro, Somesh C. Ganguli, Peter Liljeroth, and Jose L. Lado, “Moiré-enabled topological superconductivity,” *Nano Letters* **22**, 328–333 (2022).
- [35] Eylon Persky, Anders V. Bjørli, Irena Feldman, Avior Almoalem, Ehud Altman, Erez Berg, Itamar Kimchi, Jonathan Ruhman, Amit Kanigel, and Beena Kalisky, “Magnetic memory and spontaneous vortices in a van der waals superconductor,” *Nature* **607**, 692–696 (2022).
- [36] Linfeng Ai, Enze Zhang, Jinshan Yang, Xiaoyi Xie, Yunkun Yang, Zehao Jia, Yuda Zhang, Shanshan Liu, Zihan Li, Pengliang Leng, Xiangyu Cao, Xingdan Sun, Tongyao Zhang, Xufeng Kou, Zheng Han, Faxian Xiu, and Shaoming Dong, “Van der waals ferromagnetic josephson junctions,” *Nature Communications* **12** (2021), 10.1038/s41467-021-26946-w.
- [37] J. M. B. Lopes dos Santos, N. M. R. Peres, and A. H. Castro Neto, “Graphene bilayer with a twist: Electronic structure,” *Phys. Rev. Lett.* **99**, 256802 (2007).
- [38] E. Suárez Morell, J. D. Correa, P. Vargas, M. Pacheco, and Z. Barticevic, “Flat bands in slightly twisted bilayer graphene: Tight-binding calculations,” *Phys. Rev. B* **82**, 121407 (2010).
- [39] R. Bistritzer and A. H. MacDonald, “Moiré bands in twisted double-layer graphene,” *Proceedings of the National Academy of Sciences* **108**, 12233–12237 (2011).
- [40] Shiang Fang and Efthimios Kaxiras, “Electronic structure theory of weakly interacting bilayers,” *Phys. Rev. B* **93**, 235153 (2016).
- [41] A. O. Sboychakov, A. L. Rakhmanov, A. V. Rozhkov, and Franco Nori, “Electronic spectrum of twisted bilayer graphene,” *Phys. Rev. B* **92**, 075402 (2015).
- [42] Yuan Cao, Valla Fatemi, Ahmet Demir, Shiang Fang, Spencer L. Tomarken, Jason Y. Luo, Javier D. Sanchez-Yamagishi, Kenji Watanabe, Takashi Taniguchi, Efthimios Kaxiras, Ray C. Ashoori, and Pablo Jarillo-Herrero, “Correlated insulator behaviour at half-filling in magic-angle graphene superlattices,” *Nature* **556**, 80–84 (2018).
- [43] Yuan Cao, Valla Fatemi, Shiang Fang, Kenji Watanabe, Takashi Taniguchi, Efthimios Kaxiras, and Pablo Jarillo-Herrero, “Unconventional superconductivity in magic-angle graphene superlattices,” *Nature* **556**, 43–50 (2018).
- [44] Matthew Yankowitz, Shaowen Chen, Hryhorii Polshyn, Yuxuan Zhang, K. Watanabe, T. Taniguchi, David Graf, Andrea F. Young, and Cory R. Dean, “Tuning superconductivity in twisted bilayer graphene,” *Science* **363**, 1059–1064 (2019).
- [45] Xiaobo Lu, Petr Stepanov, Wei Yang, Ming Xie, Mohammed Ali Aamir, Ipsita Das, Carles Urgell, Kenji Watanabe, Takashi Taniguchi, Guangyu Zhang, Adrian Bachtold, Allan H. MacDonald, and Dmitri K. Efetov, “Superconductors, orbital magnets and correlated states in magic-angle bilayer graphene,” *Nature* **574**, 653–657 (2019).
- [46] Guorui Chen, Aaron L. Sharpe, Patrick Gallagher, Ilan T. Rosen, Eli J. Fox, Lili Jiang, Bosai Lyu, Hongyuan Li, Kenji Watanabe, Takashi Taniguchi, Jeil Jung, Zhiwen Shi, David Goldhaber-Gordon, Yuanbo Zhang, and Feng Wang, “Signatures of tunable superconductivity in a trilayer graphene moiré superlattice,” *Nature* **572**, 215–219 (2019).
- [47] Harpreet Singh Arora, Robert Polski, Yiran Zhang, Alex Thomson, Youngjoon Choi, Hyunjin Kim, Zhong Lin, Ilham Zaky Wilson, Xiaodong Xu, Jiun-Haw Chu, Kenji Watanabe, Takashi Taniguchi, Jason Alicea, and Steven Nadj-Perge, “Superconductivity in metallic twisted

- bilayer graphene stabilized by WSe₂,” *Nature* **583**, 379–384 (2020).
- [48] Yuan Cao, Jeong Min Park, Kenji Watanabe, Takashi Taniguchi, and Pablo Jarillo-Herrero, “Pauli-limit violation and re-entrant superconductivity in moiré graphene,” *Nature* **595**, 526–531 (2021).
- [49] A.L. Sharpe, E.J. Fox, A.W. Barnard, J. Finney, K. Watanabe, T. Taniguchi, M.A. Kastner, and D. Goldhaber-Gordon, “Emergent ferromagnetism near three-quarters filling in twisted bilayer graphene,” *Science* **365**, 605 (2019).
- [50] Yonglong Xie, Andrew T. Pierce, Jeong Min Park, Daniel E. Parker, Eslam Khalaf, Patrick Ledwith, Yuan Cao, Seung Hwan Lee, Shaowen Chen, Patrick R. Forrester, Kenji Watanabe, Takashi Taniguchi, Ashvin Vishwanath, Pablo Jarillo-Herrero, and Amir Yacoby, “Fractional chern insulators in magic-angle twisted bilayer graphene,” *Nature* **600**, 439–443 (2021).
- [51] Dillon Wong, Kevin P. Nuckolls, Myungchul Oh, Biao Lian, Yonglong Xie, Sangjun Jeon, Kenji Watanabe, Takashi Taniguchi, B. Andrei Bernevig, and Ali Yazdani, “Cascade of electronic transitions in magic-angle twisted bilayer graphene,” *Nature* **582**, 198–202 (2020).
- [52] U. Zondiner, A. Rozen, D. Rodan-Legrain, Y. Cao, R. Queiroz, T. Taniguchi, K. Watanabe, Y. Oreg, F. von Oppen, Ady Stern, E. Berg, P. Jarillo-Herrero, and S. Ilani, “Cascade of phase transitions and dirac revivals in magic-angle graphene,” *Nature* **582**, 203–208 (2020).
- [53] Yu Saito, Fangyuan Yang, Jingyuan Ge, Xiaoxue Liu, Takashi Taniguchi, Kenji Watanabe, J. I. A. Li, Erez Berg, and Andrea F. Young, “Isospin pomeranchuk effect in twisted bilayer graphene,” *Nature* **592**, 220–224 (2021).
- [54] A. Datta, M.J. Calderón, A. Camjayi, and E. Bascones, “Heavy quasiparticles and cascades without symmetry breaking in twisted bilayer graphene,” (2023), [arXiv:2301.13024](https://arxiv.org/abs/2301.13024), *Nature Communications* in press.
- [55] Maryam Khosravian and Jose L. Lado, “Impurity-induced excitations in a topological two-dimensional ferromagnet/superconductor van der waals moiré heterostructure,” *Phys. Rev. Mater.* **6**, 094010 (2022).
- [56] Muhammad Sufyan Ramzan, Zachary A. H. Goodwin, Arash A. Mostofi, Agnieszka Kuc, and Johannes Lischner, “Effect of coulomb impurities on the electronic structure of magic angle twisted bilayer graphene,” *npj 2D Materials and Applications* **7** (2023), [10.1038/s41699-023-00403-2](https://doi.org/10.1038/s41699-023-00403-2).
- [57] Alejandro Lopez-Bezanilla and J. L. Lado, “Defect-induced magnetism and yu-shiba-rusinov states in twisted bilayer graphene,” *Phys. Rev. Materials* **3**, 084003 (2019).
- [58] Aline Ramires and Jose L. Lado, “Impurity-induced triple point fermions in twisted bilayer graphene,” *Phys. Rev. B* **99**, 245118 (2019).
- [59] Lucas Baldo, Tomas Löthman, Patric Holmvall, and Anica M. Black-Schaffer, “Defect-induced band restructuring and length scales in twisted bilayer graphene,” *arXiv e-prints*, [arXiv:2304.03018](https://arxiv.org/abs/2304.03018) (2023), [arXiv:2304.03018](https://arxiv.org/abs/2304.03018) [cond-mat.mes-hall].
- [60] Thomas Naimier, Klaus Zollner, Martin Gmitra, and Jaroslav Fabian, “Twist-angle dependent proximity induced spin-orbit coupling in graphene/transition metal dichalcogenide heterostructures,” *Phys. Rev. B* **104**, 195156 (2021).
- [61] Klaus Zollner and Jaroslav Fabian, “Bilayer graphene encapsulated within monolayers of ws₂ or cr₂ge₂te₆: Tunable proximity spin-orbit or exchange coupling,” *Phys. Rev. B* **104**, 075126 (2021).
- [62] Petra Högl, Tobias Frank, Klaus Zollner, Denis Kochan, Martin Gmitra, and Jaroslav Fabian, “Quantum anomalous hall effects in graphene from proximity-induced uniform and staggered spin-orbit and exchange coupling,” *Phys. Rev. Lett.* **124**, 136403 (2020).
- [63] Xiangting Hu, Ning Mao, Hao Wang, Ying Dai, Baibiao Huang, and Chengwang Niu, “Quantum spin hall effect in antiferromagnetic topological heterobilayers,” *Phys. Rev. B* **103**, 085109 (2021).
- [64] Bogdan Karpiak, Aron W Cummings, Klaus Zollner, Marc Vila, Dmitrii Khokhriakov, Anamul Md Hoque, André Dankert, Peter Svedlindh, Jaroslav Fabian, Stephan Roche, and Saroj P Dash, “Magnetic proximity in a van der waals heterostructure of magnetic insulator and graphene,” *2D Materials* **7**, 015026 (2019).
- [65] C.W.J. Beenakker, “Search for majorana fermions in superconductors,” *Annual Review of Condensed Matter Physics* **4**, 113–136 (2013).
- [66] Jason Alicea, “New directions in the pursuit of majorana fermions in solid state systems,” *Reports on Progress in Physics* **75**, 076501 (2012).
- [67] Jian Li, Titus Neupert, Zhijun Wang, A. H. MacDonald, A. Yazdani, and B. Andrei Bernevig, “Two-dimensional chiral topological superconductivity in shiba lattices,” *Nature Communications* **7** (2016), [10.1038/ncomms12297](https://doi.org/10.1038/ncomms12297).
- [68] Joel Röntynen and Teemu Ojanen, “Topological superconductivity and high chern numbers in 2d ferromagnetic shiba lattices,” *Phys. Rev. Lett.* **114**, 236803 (2015).
- [69] Gerbold C. Ménard, Sébastien Guissart, Christophe Brun, Raphaël T. Leriche, Mircea Trif, François Debontridder, Dominique Demaille, Dimitri Roditchev, Pascal Simon, and Tristan Cren, “Two-dimensional topological superconductivity in pb/co/si(111),” *Nature Communications* **8** (2017), [10.1038/s41467-017-02192-x](https://doi.org/10.1038/s41467-017-02192-x).
- [70] Kim Pöyhönen, Isac Sahlberg, Alex Westström, and Teemu Ojanen, “Amorphous topological superconductivity in a shiba glass,” *Nature Communications* **9** (2018), [10.1038/s41467-018-04532-x](https://doi.org/10.1038/s41467-018-04532-x).
- [71] We take $\lambda_R = 0.2t$ for all calculations.
- [72] P. G. De Gennes, *Superconductivity of Metals and Alloys* (CRC Press, 2018).
- [73] Valerii Kachin, Teemu Ojanen, Jose L. Lado, and Timo Hyart, “Effects of electron-electron interactions in the yu-shiba-rusinov lattice model,” *Phys. Rev. B* **107**, 174522 (2023).
- [74] A. I. Buzdin, “Proximity effects in superconductor-ferromagnet heterostructures,” *Rev. Mod. Phys.* **77**, 935–976 (2005).
- [75] J L Lado and J Fernández-Rossier, “Unconventional yu-shiba-rusinov states in hydrogenated graphene,” *2D Materials* **3**, 025001 (2016).
- [76] Guangze Chen and J. L. Lado, “Impurity-induced resonant spinon zero modes in dirac quantum spin liquids,” *Phys. Rev. Research* **2**, 033466 (2020).
- [77] Maryam Khosravian and Jose L. Lado, “Impurity-induced excitations in a topological two-dimensional ferromagnet/superconductor van der waals moiré heterostructure,” *Phys. Rev. Mater.* **6**, 094010 (2022).
- [78] We take $\Lambda = 4a$, with a the lattice constant in our cal-

- culations.
- [79] Diederik P. Kingma and Jimmy Ba, “Adam: A Method for Stochastic Optimization,” *arXiv e-prints*, [arXiv:1412.6980](https://arxiv.org/abs/1412.6980) (2014), [arXiv:1412.6980 \[cs.LG\]](https://arxiv.org/abs/1412.6980).
- [80] Yann LeCun, Yoshua Bengio, and Geoffrey Hinton, “Deep learning,” *nature* **521**, 436–444 (2015).
- [81] Hiroyuki Fujita, Yuya O. Nakagawa, Sho Sugiura, and Masaki Oshikawa, “Construction of hamiltonians by supervised learning of energy and entanglement spectra,” *Phys. Rev. B* **97**, 075114 (2018).
- [82] D. Carvalho, N. A. García-Martínez, J. L. Lado, and J. Fernández-Rossier, “Real-space mapping of topological invariants using artificial neural networks,” *Phys. Rev. B* **97**, 115453 (2018).
- [83] Joaquin F. Rodriguez-Nieva and Mathias S. Scheurer, “Identifying topological order through unsupervised machine learning,” *Nature Physics* **15**, 790–795 (2019).
- [84] Mathias S. Scheurer and Robert-Jan Slager, “Unsupervised machine learning and band topology,” *Phys. Rev. Lett.* **124**, 226401 (2020).
- [85] N. L. Holanda and M. A. R. Griffith, “Machine learning topological phases in real space,” *Phys. Rev. B* **102**, 054107 (2020).
- [86] Niklas Käming, Anna Dawid, Korbinian Kottmann, Maciej Lewenstein, Klaus Sengstock, Alexandre Dauphin, and Christof Weitenberg, “Unsupervised machine learning of topological phase transitions from experimental data,” *Machine Learning: Science and Technology* **2**, 035037 (2021).
- [87] Marcello D. Caio, Marco Caccin, Paul Baireuther, Timo Hyart, and Michel Fruchart, “Machine learning assisted measurement of local topological invariants,” *arXiv e-prints*, [arXiv:1901.03346](https://arxiv.org/abs/1901.03346) (2019), [arXiv:1901.03346 \[cond-mat.dis-nn\]](https://arxiv.org/abs/1901.03346).
- [88] A. V. Balatsky, I. Vekhter, and Jian-Xin Zhu, “Impurity-induced states in conventional and unconventional superconductors,” *Rev. Mod. Phys.* **78**, 373–433 (2006).
- [89] Michael Ruby, Falko Pientka, Yang Peng, Felix von Oppen, Benjamin W. Heinrich, and Katharina J. Franke, “End states and subgap structure in proximity-coupled chains of magnetic adatoms,” *Phys. Rev. Lett.* **115**, 197204 (2015).
- [90] Howon Kim, Alexandra Palacio-Morales, Thore Posske, Levente Rózsa, Krisztián Palotás, László Szunyogh, Michael Thorwart, and Roland Wiesendanger, “Toward tailoring majorana bound states in artificially constructed magnetic atom chains on elemental superconductors,” *Science Advances* **4** (2018), [10.1126/sciadv.aar5251](https://doi.org/10.1126/sciadv.aar5251).
- [91] Benjamin E. Feldman, Mallika T. Randeria, Jian Li, Sangjun Jeon, Yonglong Xie, Zhijun Wang, Ilya K. Drozdov, B. Andrei Bernevig, and Ali Yazdani, “High-resolution studies of the majorana atomic chain platform,” *Nature Physics* **13**, 286–291 (2016).
- [92] Laëtitia Farinacci, Gelavizh Ahmadi, Gaël Reecht, Michael Ruby, Nils Bogdanoff, Olof Peters, Benjamin W. Heinrich, Felix von Oppen, and Katharina J. Franke, “Tuning the coupling of an individual magnetic impurity to a superconductor: Quantum phase transition and transport,” *Phys. Rev. Lett.* **121**, 196803 (2018).
- [93] Lucas Schneider, Philip Beck, Thore Posske, Daniel Crawford, Eric Mascot, Stephan Rachel, Roland Wiesendanger, and Jens Wiebe, “Topological shiba bands in artificial spin chains on superconductors,” *Nature Physics* **17**, 943–948 (2021).
- [94] Andreas Theiler, Kristofer Björnson, and Annica M. Black-Schaffer, “Majorana bound state localization and energy oscillations for magnetic impurity chains on conventional superconductors,” *Phys. Rev. B* **100**, 214504 (2019).
- [95] Mahdi Mashkoori, Saurabh Pradhan, Kristofer Björnson, Jonas Fransson, and Annica M. Black-Schaffer, “Identification of topological superconductivity in magnetic impurity systems using bulk spin polarization,” *Phys. Rev. B* **102**, 104501 (2020).